Supplementary Information for

Decoding Molecular Water Structure at Complex Interfaces through Surface-Specific Spectroscopy of the Water Bending Mode

Takakazu Seki,[1,#] Chun-Chieh Yu,[1,#] Xiaoqing Yu,[1] Tatsuhiko Ohto,[2] Shumei Sun,[1,3,4] Konrad Meister,[1,5] Ellen H. G. Backus,[1,4] Mischa Bonn,[1,] and Yuki Nagata[1,*]*

1. Max Planck Institute for Polymer Research, Ackermannweg 10, 55128, Mainz, Germany

2. Graduate School of Engineering Science, Osaka University, 1-3 Machikaneyama, Toyonaka, Osaka 560-8531, Japan

3. Applied Optics Beijing Area Major Laboratory, Department of Physics, Beijing Normal University, Beijing 100875, China

4. Department of Physical Chemistry, University of Vienna, Währinger Strasse 42, 1090 Vienna, Austria

5. Department of Natural Sciences, University of Alaska Southeast, Juneua, Alaska 99801, United States

[*]Correspondence: bonn@mpip-mainz.mpg.de, nagata@mpip-mainz.mpg.de

[#]These authors contributed equally

SFG Setup

SFG measurements were performed on a femtosecond Ti: Sapphire amplified laser system (Coherent Libra, ~800 nm, ~50 fs, 1 kHz) with 5 W output power. We used 2 W to pump an optical parametric amplifier (TOPAS, light conversion) with a noncollinear DFG stage to generate the broadband IR pulse. Another 1 W of the laser output was passed through an etalon to generate the narrowband visible pulse (~20 cm^{-1}). The visible and IR beams overlapped spatially and temporally at the sample surface with their incident angles of 64° and 40° with respect to the surface normal, respectively. Subsequently, the SFG signal is dispersed in a spectrometer and detected by an EMCCD camera. The visible and IR beams had

pulse energies of roughly 20 μJ and 1 μJ, respectively, at the sample position. All spectra were collected in the *ssp* (denoting *s*-, *s*-, and *p*-polarized SFG, visible and IR, respectively) polarization combination.

SFG Measurement at the Water-Air Interface

For the isotopic dilution experiments, we prepared H_2O/D_2O mixture solutions with various ratio, H_2O/D_2O=1/0, 2/1, 1/1, 1/2, and 0/1. H_2O is ultra-pure water from a MilliQ machine (18.2 MΩ cm). D_2O (>99.9%) was purchased from Eurisotop and used as received. We poured the solution into a rotating trough and measured the H-O-H bending mode signals for 15 × 20 min at the water-air interface with the rotating trough (11 rpm, 8 cm in a diameter). To avoid the effect of water vapor absorption of IR, we started the measurements after flushing with N_2 for 7.5 min. The spectra for water-air were normalized to the non-resonant signal taken from *z*-cut quartz after subtracting a background spectrum.

SFG Measurement at the Water-CaF$_2$ Interface

The low and high pH solutions were prepared by diluting HCl or NaOH with NaCl aqueous solution to the corresponding pH solutions used in this work. For instance, the high (low) pH solution with a pH of roughly 12 ± 0.5 (2 ± 0.5) was obtained by diluting NaOH (HCl) in NaCl aqueous solution down to a concentration of 0.01 M for NaOH (HCl) and 0.1 M for NaCl. Here, we would like to note that the $\chi^{(3)}$ contribution is crucial at charged interfaces. As is widely accepted, high concentration of salt screens the $\chi^{(3)}$ contribution. Therefore, to suppress the $\chi^{(3)}$ contribution, we added NaCl salt into the water-CaF$_2$ system. A previous report shows that above 0.1 M of NaCl, the spectral feature is unchanged.[1]

Before use, a fluorite window was soaked in saturated CaF$_2$ aqueous solution overnight to reconstruct the CaF$_2$ surface. Subsequently, we cleaned the CaF$_2$ window with Ar-plasma treatment for 10 minutes to remove organic contaminants, and generate the fresh surface by facilitating dissolution of CaF$_2$ under HCl solution at pH 2 for 2-3 hours. A similar treatment was also used in the previous studies[2,3] Then, we measured the H-O-H bending mode signals for 8 × 5 min at the water-CaF$_2$ interface after flushing with N_2 for 7.5 min. We

would like to note that for water-CaF$_2$ interface to avoid position specificity as much as possible we measured eight different positions by rotating CaF$_2$ window around its surface normal with 45 degree for each measurement and averaged these spectra. For stretch mode measurements of water-CaF$_2$, we measured the SFG signal for 8 × 2 min in a similar manner to the bending mode measurements for water-CaF$_2$ and combined three different frequency regions to obtain the whole spectra shown in Fig. 3(b). To avoid vibrational coupling effects, we used isotopically diluted water with mixture ratio of H$_2$O/D$_2$O = 1/2. The spectra for water-CaF$_2$ were normalized to the non-resonant signal taken from gold-CaF$_2$ interface after subtracting a background spectrum.

SFG Measurement at the Water-Air Interface in the Presence of HSA

We dissolved HSA powder (Sigma Aldrich) into pure D$_2$O solution at a concentration of 10 µM. Then, we poured 20 mL of the isotopically diluted water with various H$_2$O/D$_2$O mixture ratio (H$_2$O/D$_2$O = 1/0, 3/1, 1/1, 1/3, and 0/1.) into a rotating trough. To generate an HSA layer on water, we added a controlled amount (25 µL) of the HSA solution onto the isotopically diluted water using a click syringe. The final concentration of HSA was adjusted to be 0.0125 µM. The isoelectric point of HSA in bulk water is pH=5.1[4]. Since we have used the Milli-Q water (pH~6.0), it is reasonable to assume that the protein is not strongly charged. As such, the $\chi^{(3)}$ contribution for the water at the protein-water interface is negligibly small. Since the strong amide I mode overlaps with the H-O-H bending mode, we focused on the H-O-D bending mode. After flushing with N$_2$ for 20 min, we measured the H-O-D bending mode signals for 20 min at the water-HSA interface with the rotating trough (11 rpm, 8 cm in a diameter) [5] to avoid excess heating effects of the sample by laser irradiation. The measured spectra were normalized to the non-resonant signal taken from z-cut quartz after subtracting a background spectrum. Similarly, the C-H stretch region was measured for 2 x 10 min as shown in Fig. S1. Peak signatures at ~2860 cm^{-1} and ~2920 cm^{-1} are mostly attributed to symmetric and anti-symmetric C-H stretch mode of CH$_3$ groups, and a peak at ~3050 cm^{-1} is attributed to an aromatic C-H stretch mode of the proteins. Based on these observed vibrational signatures, we confirmed that HSA protein was present at the water-air interface even at such low concentration of protein.
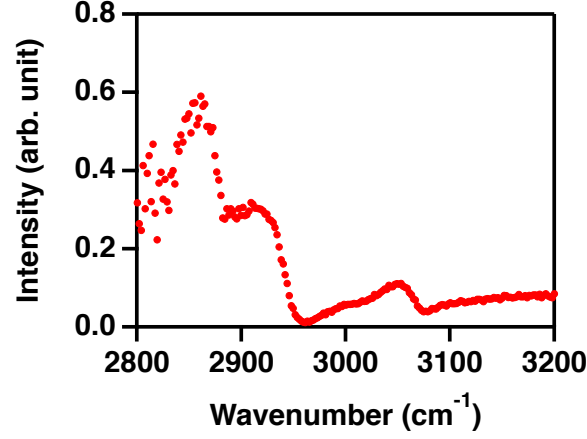
Fig. S1 SFG spectrum in the C-H stretch region obtained at the water-air interface in the presence of HSA protein.

Fitting Procedure for SFG Spectra of the Water Bending Mode at the Water-air Interface

We performed the spectral fitting for the SFG spectra at H_2O-air and D_2O-air interfaces via;

$$\left|\chi_{\text{eff}}^{(2)}(\omega)\right|^2 = \left|A_{NR}e^{i\phi_{NR}} + \chi_{\text{bend1}}^{(2)}(\omega) + \chi_{\text{bend2}}^{(2)}(\omega)\right|^2$$

$$(S1)$$

and

$$|\chi_{\text{eff}}^{(2)}(\omega)|^2 = |A_{NR}e^{i\phi_{NR}} + \chi_{\text{OD-str}}^{(2)}(\omega)|^2,$$

$$(S2)$$

respectively. For the fitting, we assumed the Lorentzian model to describe the vibrational modes as

$$\chi_{\text{bend1}}^{(2)}(\omega) = \frac{A_{\text{bend1}}}{\omega - \omega_{\text{bend1}} + i\Gamma_{\text{bend1}}},$$

$$(S3)$$

$$\chi_{\text{bend2}}^{(2)}(\omega) = \frac{A_{\text{bend2}}}{\omega - \omega_{\text{bend2}} + i\Gamma_{\text{bend2}}},$$

$$(S4)$$

and

$$\chi^{(2)}_{\text{OD-str}}(\omega) \; = \; \frac{A_{\text{OD}}}{\omega - \omega_{\text{OD}} + i\Gamma_{OD}}.$$

(S5)

For the H_2O-air interface, we use two Lorentzians, which represent the bending modes of the water molecules with two hydrogen-bond donors (DD) and with one donor and the other free OH group (D).[6–9] Based on parameters previously obtained in ref. 10., we made constraints for Eq. (S3) and (S4), $\Gamma_{\text{bend1}} = \Gamma_{\text{bend2}} = 65$, $\omega_{\text{bend1}} = 1612$, and $\omega_{\text{bend2}} = 1661$, where the units of Γ and ω are cm^{-1}. We also constrained $\omega_{\text{O-D}}$ and $\Gamma_{\text{O-D}}$ as 2397 cm^{-1} and 73 cm^{-1}, respectively, which were independently determined by fitting hydrogen-bonded O-D stretch region for the D_2O-air interface. The phase of the non-resonant contribution (ϕ_{NR}) was constrained to have the same value for fitting the spectra. Through this fit, we obtained $A_{\text{bend1}} = 1.2$ and $A_{\text{O-D}} = 80.2$. For fitting the other isotopic dilution composition, we used three Lorentzians (Eq. S6) with constraints on the bending mode contribution of D-type water and O-D stretch contribution by considering the mole fraction of H-O-H chromophore [HOH] and O-D stretch chromophore [OD] calculated based on the equilibrium constant of 3.86 for $H_2O + D_2O \rightleftarrows 2HDO$.[11–13]

$$\left|\chi^{(2)}_{\text{eff}}(\omega)\right|^2 = \left|A_{NR}e^{i\phi_{NR}} + \chi^{(2)}_{\text{bend1}}(\omega) + \chi^{(2)}_{\text{bend2}}(\omega) + [OD]\chi^{(2)}_{\text{OD-str}}(\omega)\right|^2$$

(S6)

Similarly, by making constraints on $\omega_{\text{O-D}}$, $\Gamma_{\text{O-D}}$, and ϕ_{NR}, we performed global fitting. The phase of the non-resonant contribution (ϕ_{NR}) was constrained to have the same value by assuming that the phase of non-resonant contribution does not change upon isotopic dilution. The fit residuals and the obtained parameters are displayed in Fig. S2 and Table S1, respectively.
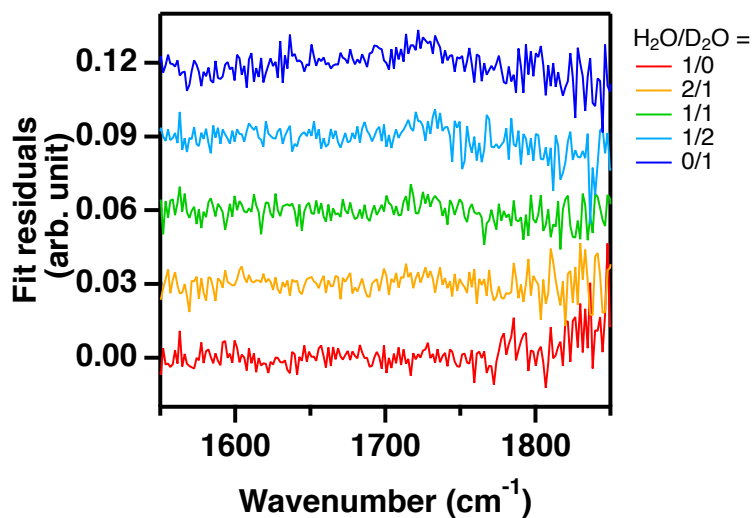
Fig. S2. The fit residual obtained from the global fitting. The residuals are offset by 0.03 for clarity.

Table S1. Fitting parameters for the vibrational SFG spectra at the water-air interface with various isotopic composition. The fitting parameters of pure H_2O and D_2O are based on the ref. 10 and O-D stretch region, respectively. For other isotopic mixtures, the bend 1 and O-D stretch contribution are assumed to linearly depend on H_2O fraction.

H_2O fraction	100%	44.7%	25.3%	11.4%	0%
A_{NR}	-0.30 ± 0.01	-0.26 ± 0.01	-0.24 ± 0.01	-0.20 ± 0.01	-0.14 ±0.01
ϕ_{NR} (rad)	-0.04±0.05	-0.04±0.05	-0.04±0.05	-0.04±0.05	-0.04±0.05
A_{bend1}	1.23	0.55	0.31	0.16	—
ω_{bend1} (cm^{-1})	1612.0	1612.0	1612.0	1612.0	—
Γ_{bend1} (cm^{-1})	65.0	65.0	65.0	65.0	—
A_{bend2}	-10.8 ± 0.4	-4.8±0.7	-2.6 ± 0.6	-1.5 ± 0.6	—
ω_{bend2} (cm^{-1})	1661.0 ± 10.4	1659.3 ± 5.9	1659.0 ± 9.4	1647.1 ± 14.9	—
Γ_{bend2} (cm^{-1})	65.0	56.3 ± 7.3	51.0 ± 3.1	48.2 ± 16.1	—
A_{O-D}	—	26.7	40.7	53.4	80.2
ω_{O-D} (cm^{-1})	—	2397	2397	2397	2397
Γ_{O-D} (cm^{-1})	—	73.0	73.0	73.0	73.0

Fitting Procedure for SFG Spectra of Water Bending Mode at Water-CaF₂ Interface

We performed the spectral fitting for the SFG spectra at water-CaF₂ interface at different pH via;

$$\left|\chi_{\text{eff}}^{(2)}(\omega)\right|^2 = \left|A_{NR}e^{i\phi_{NR}} + \chi_{\text{bend}}^{(2)}(\omega)\right|^2$$

(S7).

For the fitting, we assumed Lorentzian model to describe the vibrational modes as

$$\chi_{\text{bend}}^{(2)}(\omega) = \frac{A_{\text{bend}}}{\omega - \omega_{\text{bend}} + i\Gamma_{\text{bend}}}$$

(S8).

The phase of the non-resonant contribution (ϕ_{NR}) was constrained to have the same value for fitting the spectra by assuming that the phase of non-resonant contribution does not change upon the pH variation. The obtained parameters are displayed in Table S2.

Table S2. Fitting parameters for the vibrational SFG spectra at the water-CaF₂ interface at different pH.

H₂O fraction	pH2	pH12
A_{NR}	0.26 ± 0.02	0.27 ± 0.02
ϕ_{NR} (rad)	-0.29 ± 0.05	-0.29 ± 0.05
A_{bend}	12.1 ± 1.0	-12.1 ± 0.8
ω_{bend} (cm⁻¹)	1632.6 ± 1.2	1661.9 ± 2.5
Γ_{bend} (cm⁻¹)	48.0 ± 1.7	76.5 ± 4.0

Fitting Procedure for SFG Spectra of O-H stretch Mode at Water-CaF₂ Interface

We performed the spectral fitting for the SFG spectra at water-CaF₂ interface at different pH via;

$$\left|\chi_{\text{eff}}^{(2)}(\omega)\right|^2 = \left|A_{NR}e^{i\phi_{NR}} + \chi_{\text{OH1}}^{(2)}(\omega) + \chi_{\text{OH2}}^{(2)}(\omega)\right|^2$$

(S9).

For the fitting, we assumed Lorentzian model to describe the vibrational modes as

$$\chi_{\text{OH1}}^{(2)}(\omega) = \frac{A_{\text{OH1}}}{\omega - \omega_{\text{OH1}} + i\Gamma_{\text{OH1}}}$$

(S10)

and

$$\chi_{\text{OH2}}^{(2)}(\omega) = \frac{A_{\text{OH2}}}{\omega - \omega_{\text{OH2}} + i\Gamma_{\text{OH2}}}$$

(S11).

The phase of the non-resonant contribution (ϕ_{NR}) was constrained to have the same value for fitting the spectra by assuming that the phase of non-resonant contribution does not change upon the pH variation. The obtained parameters are displayed in Table S3. The lower frequency contribution at pH2 is assumed to be the residual coupling contribution in O-H stretch region. Here, we would like to note that because the O-H stretch mode is much stronger than the non-resonant contribution unlike the H-O-H bending mode, the non-resonant contribution is nearly zero for the O-H stretch spectra, in particular at pH2, while the non-resonant contribution is certainly large for the H-O-H bending mode spectra.

Table S3. Fitting parameters for the vibrational SFG spectra at the water-CaF$_2$ interface at different pH.

H$_2$O fraction	pH 2	pH 12
A_{NR}	-0.01 ± 0.01	0.12 ± 0.01
ϕ_{NR} (rad)	-0.16 ± 0.09	-0.16 ± 0.09
A_{OH1}	10.5 ± 2.2	12.6 ± 0.5
ω_{OH1} (cm^{-1})	3425.9 ± 2.9	3654.6 ±1.8
Γ_{OH1} (cm^{-1})	86.9 ± 6.6	49.0 ± 1.9
A_{OH2}	25.5 ± 2.7	-49.8 ± 3.4
ω_{OH2} (cm^{-1})	3320.1 ± 5.5	3362.7 ± 14.6
Γ_{OH2} (cm^{-1})	134.6 ± 5.1	279.3 ± 10.7

Fitting Procedure for SFG Spectra of the Water Bending Mode at the Water-Air interface in the presence of HSA

Firstly, to extract the interfacial water contribution from complex protein contributions, we performed the spectral fitting for the SFG spectra at H$_2$O-air, H$_2$O/D$_2$O mixture-air, and D$_2$O-air interfaces in the presence of HSA via:

$$\left|\chi_{\text{eff}}^{(2)}(\omega)\right|^2 = \left|A_{NR}e^{i\phi_{NR}} + \chi_{\text{HSA1}}^{(2)}(\omega) + \chi_{\text{HSA2}}^{(2)}(\omega) + \chi_{\text{HOD\_bend}}^{(2)}(\omega)\right|^2.$$

(S12)

For the fitting, we assumed Lorentzian model to describe the protein features of the signal around 1410 cm^{-1} ($\chi_{\text{HSA1}}^{(2)}$), the signal around 1500-1550 cm^{-1} ($\chi_{\text{HSA2}}^{(2)}$), and H-O-D contribution as

$$\chi_{\text{HSA1/2}}^{(2)}(\omega) = \frac{A_{\text{HSA1/2}}}{\omega - \omega_{\text{HSA1/2}} + i\Gamma_{\text{HSA1/2}}},$$

(S13)

and

$$\chi_{\text{HOD\_bend}}^{(2)}(\omega) = \frac{A_{\text{HOD\_bend}}}{\omega - \omega_{\text{HOD\_bend}} + i\Gamma_{\text{HOD\_bend}}},$$

(S14)

respectively. First, to describe protein features, we performed the spectral fitting for the SFG spectra at H_2O-air and D_2O-air interfaces. The phase of the non-resonant contribution (ϕ_{NR}) was constrained to have the same value for fitting the spectra by assuming that the phase of non-resonant contribution does not change upon isotopic dilution. The obtained parameters are displayed in Table S4.

Table S4. Fitting parameters for the vibrational SFG spectra at the water-air interface in the presence of HSA.

H_2O fraction	100%	0%
A_{NR}	0.14 ± 0.01	0.10 ± 0.01
ϕ_{NR} (rad)	-0.48 ± 0.05	-0.48 ± 0.05
A_{HSA1}	7.1 ± 0.5	6.4 ± 0.4
ω_{HSA1} (cm^{-1})	1416.4 ± 1.4	1410.8 ± 0.9
Γ_{HSA1} (cm^{-1})	30.2 ± 1.3	24.7 ± 1.0
A_{HSA2}	1.1 ± 0.3	0.9 ± 0.3
ω_{HSA2} (cm^{-1})	1513.6 ± 2.2	1519.0 ± 3.1
Γ_{HSA2} (cm^{-1})	21.8 ± 5.5	20.0 ± 6.2

Based on these fitting parameters for HSA contributions, we further performed the spectral fitting to extract H-O-D contribution for the SFG spectra at H_2O-air, H_2O/D_2O mixture-air, and D_2O-air interfaces with HSA via Eq. (S12). Here, we assumed the protein contributions (amplitude and frequency) are linearly variated depending on H/D mixture ratio from 100% to 0%. The phase of the non-resonant contribution (ϕ_{NR}) was constrained to have the same value for fitting the spectra by assuming that the phase of non-resonant contribution does not change upon isotopic dilution. For H-O-D bending contributions, the $\omega_{\mathrm{HOD\_bend}}$ and $\Gamma_{\mathrm{HOD\_bend}}$ were set to be the same for fitting the spectra because the intermolecular coupling between bending modes of interfacial water is negligibly small. The obtained parameters are displayed in Table S5.

Table S5. Fitting parameters for the vibrational SFG spectra at the water-air interfaces in the presence of HSA with various ratio of H_2O and D_2O. The HSA parameters of pure H_2O and D_2O are based on the Table S4. For other isotopic mixture, the HSA contributions are assumed to linearly depend on H_2O fraction.

H_2O fraction	100%	44.7%	25.3%	11.4%	0%
A_{NR}	0.14 ± 0.01	0.15 ± 0.01	0.13 ± 0.01	0.10 ± 0.01	0.10 ± 0.01
ϕ_{NR} (rad)	-0.47 ± 0.01	-0.47 ± 0.01	-0.47 ± 0.01	-0.47 ± 0.01	-0.47 ± 0.01
A_{HSA1}	7.1	6.9	6.7	6.6	6.4
ω_{HSA1} (cm^{-1})	1416.4	1415.0	1413.6	1412.2	1410.8
Γ_{HSA1} (cm^{-1})	30.1 ± 0.5	30.9 ± 0.5	31.5 ± 0.6	31.5 ± 0.6	24.6 ± 0.3
A_{HSA2}	1.1	1.0	1.0	0.9	0.9
ω_{HSA2} (cm^{-1})	1513.6	1515.0	1516.3	1517.7	1519.0
Γ_{HSA2} (cm^{-1})	21.3 ± 1.8	26.1 ± 4.6	34.5 ± 13.8	33.7 ± 12.0	20.3 ± 2.6
A_{HOD_bend}	——	1.7 ± 0.3	3.2 ± 0.5	2.6 ± 0.5	——
ω_{HOD_bend} (cm^{-1})	——	1506.0 ± 3.0	1506.0 ± 3.0	1506.0 ± 3.0	——
Γ_{HOD_bend} (cm^{-1})	——	42.0 ± 7.0	42.0 ± 7.0	42.0 ± 7.0	——

SFG Spectra Calculation for the Water Bending Mode via Surface-Specific Cross-Correlation Formalism

We computed the SFG spectra of water at the water-air interface by using the AIMD trajectories obtained from ref. 14. In short, the systems used in the AIMD simulations contained 160 D_2O molecules in a 16.63 x 16.63 x 44.1 cell. We used the B3LYP-D3(0) and revPBE0-D3(0) levels of theory for the AIMD simulation. The auxiliary density matrix method was used to accelerate the calculation of Hartree-Fock exchange.[15] The trajectories have a total length of 160 ps. The obtained vibrational frequencies were corrected according to the frequency correction scheme of water vibration. The D-O-D bend frequencies were converted to the H-O-H bend frequencies by using a factor of 1/0.735. We used the scaling factors of the frequency axis of 0.985 and 0.977 for B3LYP-D3(0) and revPBE0-D3(0), respectively, which is given in ref. 16.

For computing the bending mode SFG spectra at the water-air interface, we modified the surface-specific velocity-velocity correlation function (ssVVCF) formalism;[17]

$$\chi_{xxz}^{(2),R}(\omega) = \frac{Q(\omega)\mu'\alpha'}{i\omega^2} \int_0^\infty dt e^{-i\omega t} \langle \sum_{i,j} g_{ds}(z_i(0)) g_t(r_{ij}(0); r_t) \dot{r}_{z,i}^{OM}(0) \frac{\dot{\boldsymbol{r}}_j^{OM}(t) \cdot \boldsymbol{r}_j^{OM}(t)}{|\boldsymbol{r}_j^{OM}(t)|} \rangle,$$

(S15)

where $Q(\omega)$ is the quantum correction factor, μ' (α') is transition dipole moment (polarizability), $z_i(t)$ is the *z*-coordinate of the *i*th oxygen atom at time *t*, and $g_{ds}(z_i)$ is the function for the dividing surface to selectively extract the vibrational responses of D_2O molecules near the interface. μ' and α' are not sensitive to the bending mode frequency, and thus are frequency-independent unlike the O-H stretch mode.[6] $\boldsymbol{r}_j^{OM}(t)$ is the vector pointing from the oxygen atom (O) to the middle point of the two hydrogen atoms (M) for water molecule *i* at time *t*. $g_t(r_{ij}(0); r_t)$ excludes the correlation of the different water molecules, *i* and *j*, when the oxygen-oxygen distance of water molecules *i* and *j* ($r_{ij}(0)$) is larger than the cutoff distance r_t.[18]

Here, we would like to note that previously Khatib and Sulpizi computed the water bending mode spectra at the water-air interface by using the AIMD trajectories at the BLYP-D3(0) level of theory.[19] Their spectrum showed a positive $\text{Im}(\chi^{(2)})$ feature, unlike the positive and negative feature we obtained in this work. This difference can be attributed to the different formulation of the ssVVCF. In the current study, we formulated the ssVVCF based on the H-O-H bending motion for computing the bending mode SFG spectra, while their spectral calculation employed the formulation based on the O-H stretch motion. In fact, when we computed the ssVVCF SFG spectra based on the O-H stretch motion,[17]

$$\chi_{xxz}^{(2),R}(\omega) = \frac{Q(\omega)\mu'\alpha'}{i\omega^2} \int_0^\infty dt e^{-i\omega t} \langle \sum_{i,j} g_{ds}(z_i(0)) g_t(r_{ij}(0); r_t) \dot{r}_{z,i}^{OD}(0) \frac{\dot{\boldsymbol{r}}_j^{OD}(t) \cdot \boldsymbol{r}_j^{OD}(t)}{|\boldsymbol{r}_j^{OD}(t)|} \rangle,$$

(S16)

the spectrum showed a positive feature (see Fig. S3). Thus, to compute the SFG spectra of the bending mode via the ssVVCF formalism, one needs to use the formalism for the bending motion.
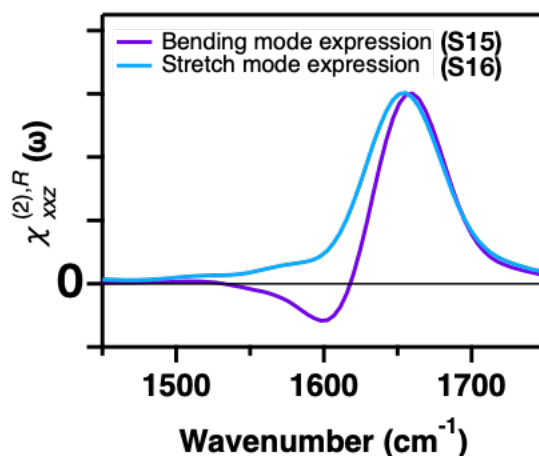
Fig. S3 SFG spectra calculated at the revPBE0-D3(0) level of theory with Eqs. (S15) and (S16) for the H-O-H bending and O-H stretch motions, respectively. r_t was set to 0, meaning that only autocorrelation functions are considered.

References

1   P. A. Covert, K. C. Jena and D. K. Hore, Throwing Salt into the Mix: Altering Interfacial Water Structure by Electrolyte Addition, *J. Phys. Chem. Lett.*, 2014, **5**, 143–148.

2   S. Schrödle and G. L. Richmond, Equilibrium and non-equilibrium kinetics of self-assembled surfactant monolayers: A vibrational sum-frequency study of dodecanoate at the fluorite-water interface, *J. Am. Chem. Soc.*, 2008, **130**, 5072–5085.

3   K. A. Becraft, F. G. Moore and G. L. Richmond, In-situ spectroscopic investigations of surfactantadsorption and water structure at the CaF 2 /aqueous solution interface, *Phys. Chem. Chem. Phys.*, 2004, **6**, 1880–1889.

4   B. Jachimska, M. Wasilewska and Z. Adamczyk, Characterization of Globular Protein Solutions by Dynamic Light Scattering, Electrophoretic Mobility, and Viscosity Measurements, *Langmuir*, 2008, **24**, 6866–6872.

5   E. H. G. Backus, D. Bonn, S. Cantin, S. Roke and M. Bonn, Laser-heating-induced displacement of surfactants on the water surface, *J. Phys. Chem. B*, 2012, **116**, 2703–2712.

6   Y. Ni and J. L. Skinner, IR and SFG vibrational spectroscopy of the water bend in the bulk liquid and at the liquid-vapor interface, respectively, *J. Chem. Phys.*, 2015, **143**, 014502.

7   Y. Nagata, C.-S. Hsieh, T. Hasegawa, J. Voll, E. H. G. Backus and M. Bonn, Water Bending Mode at the Water–Vapor Interface Probed by Sum-Frequency Generation Spectroscopy: A Combined Molecular Dynamics Simulation and Experimental Study, *J. Phys. Chem. Lett.*, 2013, **4**, 1872–1877.

8   D. R. Moberg, S. C. Straight and F. Paesani, Temperature Dependence of the Air/Water Interface Revealed by Polarization Sensitive Sum-Frequency Generation Spectroscopy, *J. Phys. Chem. B*, 2018, **122**, 4356–4365.

9   C. Dutta and A. V. Benderskii, On the Assignment of the Vibrational Spectrum of the Water Bend at the Air/Water Interface, *J. Phys. Chem. Lett.*, 2017, **8**, 801–804.

10   T. Seki, S. Sun, K. Zhong, C. Yu, K. Machel, L. B. Dreier, E. H. G. Backus, M. Bonn and Y. Nagata, Unveiling Heterogeneity of Interfacial Water through the Water Bending Mode, *J. Phys. Chem. Lett.*, 2019, **10**, 6936–6941.

11   J. Meija, Z. Mester and A. D'Ulivo, Mass spectrometric separation and quantitation of overlapping isotopologues. H2O/HOD/D2O and H2Se/HDSe/D2Se mixtures, *J. Am. Soc. Mass Spectrom.*, 2006, **17**, 1028–1036.

12   M. Wolfsberg, A. A. Massa and J. W. Pyper, Effect of Vibrational Anharmonicity on the Isotopic Self-Exchange Equilibria H 2 X+D 2 X=2HDX, *J. Chem. Phys.*, 1970, **53**, 3138–3146.

13   J. C. Duplan, L. Mahi and J. L. Brunet, NMR determination of the equilibrium constant for the liquid H2O–D2O mixture, *Chem. Phys. Lett.*, 2005, **413**, 400–403.

14   T. Ohto, M. Dodia, J. Xu, S. Imoto, F. Tang, F. Zysk, T. D. Kühne, Y. Shigeta, M. Bonn, X. Wu and Y. Nagata, Accessing the Accuracy of Density Functional Theory through Structure and Dynamics of the Water–Air Interface, *J. Phys. Chem. Lett.*, 2019, **10**, 4914–4919.

15   M. Guidon, J. Hutter and J. VandeVondele, Auxiliary Density Matrix Methods for

Hartree–Fock Exchange Calculations, *J. Chem. Theory Comput.*, 2010, **6**, 2348–2364.

16   K. Zhong, C.-C. Yu, M. Dodia, M. Bonn, Y. Nagata and T. Ohto, Vibrational Mode Frequency Correction of Liquid Water in Density Functional Theory Molecular Dynamics Simulations with van der Waals Correction, *submitted*.

17   T. Ohto, K. Usui, T. Hasegawa, M. Bonn and Y. Nagata, Toward ab initio molecular dynamics modeling for sum-frequency generation spectra; an efficient algorithm based on surface-specific velocity-velocity correlation function, *J. Chem. Phys.*, 2015, **143**, 124702.

18   Y. Nagata and S. Mukamel, Vibrational Sum-Frequency Generation Spectroscopy at the Water/Lipid Interface: Molecular Dynamics Simulation Study, *J. Am. Chem. Soc.*, 2010, **132**, 6434–6442.

19   R. Khatib and M. Sulpizi, Sum Frequency Generation Spectra from Velocity-Velocity Correlation Functions, *J. Phys. Chem. Lett.*, 2017, **8**, 1310–1314.